2-2022

Synthesis and Evaluation of a Novel Polyacrylamide Functionalized Nano-Silica as a Calcium Carbonate Inhibitor in Upstream Applications

Nadhem Ismail

Ali Alshami
University of North Dakota, ali.alshami@und.edu

Ibnelwaleed A. Hussein

Synthesis and Evaluation of a Novel Polyacrylamide Functionalized Nano-Silica as a Calcium Carbonate Inhibitor in Upstream Applications

Nadhem Ismail[1], Ali S. Alshami[1], Ibnelwaleed A. Hussein[2]

1. University of North Dakota, Grand Forks, ND, USA.
2. Gas Processing Center, College of Engineering, Qatar University, P.O. Box 2713, Doha, Qatar

*Corresponding author email: ali.alshami@und.edu

Abstract

Calcium carbonate scale forms in production and injection wells, precipitating upon pressure and temperature changes, incompatible water mixing, and dehydration. Production shutdown is one of the most dramatic consequences caused by calcium carbonate scale formation. We synthesized, characterized, and tested a polyacrylamide functionalized nano-silica (PAM-SiO_2NPs) inhibitor that prevents calcium carbonate formation at high temperatures and high brine. Positive compatibility results were confirmed before the inhibition efficiency test, whereby the efficiency was calculated by quantifying the calcium ions left in solution using ICP-OES. The inhibitor was effective at temperatures of 40, 60, and 80 °C, with pH values of 7, and 9, and varying brine compositions. The inhibition efficiency increased with an increase in temperature and pH, reaching 95% after 16 hours of reaction time at a temperature of 80 °C, and a pH of 7 using an inhibitor concentration of 20 ppm (mg/l). A higher amount of scale formed due to an abundance of calcium ions with a cationic to anionic ratio of 80/20; however, the inhibition efficiency was higher with a ratio of 20/80, especially at lower inhibitor dosages. The collected scale in the blank and the samples with low inhibitor concentrations were characterized using SEM/EDS and TEM. The Characterization indicated that the inhibitor chelates calcium, preventing scale formation. SEM results indicated a change in scale morphology as the inhibitor was absorbed to the active crystal

sites, interrupting the microcrystal growth. These findings indicate promising inhibition results at high temperatures, varying pH values, and different brine concentrations with relatively low inhibitor concentrations. Results were compared to commercial inhibitors and found to be more effective (> 80%) at very low concentrations (0.2 ppm).

Keywords: polyacrylamide functionalized nano-silica; oil production; inhibitor efficiency; calcium carbonate chelates; oilfield scales; calcite.

1. Introduction

Calcium carbonate is one of the most frequently occurring scales in the oil and gas industry especially in deeper wells at high temperature, pressure and brine concentrations [1] [2] [3]. It forms when Ca^{2+} is supersaturated with ${CO_3}^{2-}$ or${HCO_3}^{-}$, according to Equations 1 and 2:

$$Ca^{2+}{}_{(aq)} + {CO_3}^{2-}{}_{(aq)} \rightarrow CaCO_{3(s)} \quad (1)$$

$$Ca^{2+}{}_{(aq)} + 2{HCO_3}^{-}{}_{(aq)} \rightarrow CaCO_{3(s)} + CO_{2(g)} + H_2O_{(l)} \quad (2)$$

Ion super-saturation depends on many factors and contributes to scale formation since water is produced from wells with high salt concentrations [4]. Scale formation is affected by changes in physical variables such as temperature, pressure, and pH, which determine scale type and composition[5] [6]. Contrary to other scale types, the solubility of calcium carbonate decreases at high temperature which assist precipitation earlier when high temperature is encountered. The inverse solubility behavior of calcium carbonate is explained by thermodynamic equilibrium which favors the forward reaction in (2) at high temperature, since gases such as CO_2 are less soluble in warm solutions [7], [8]. The same phenomenon occurs when pH increases. High pH leads to lower solubility; therefore, precipitation also occurs at earlier stages. Higher

concentrations of scaling ions, such as, $Ca^{2+}\ and\ CO3^{2-}$, will lead to a higher precipitation potential.

Scale formation can quickly lower production capacity to zero in just a few hours, incurring excessive treatment costs [9]. Scale deposition in formation pores blocks fluid by reducing the diameter leading to a high-pressure drop and full blockage that limits production. Scale formation causes additional problems such as energy leakage, corrosion acceleration, and severe accidents that interfere with safety and production economics [10].

Scale inhibition is the most reasonable and beneficial scale mitigation strategy in the oil and gas industry; however, this technique is challenging as it is dependent on the environment, the mixture of compounds found in the scale, the concentration of the ions present, and formation conditions [11][1]. Different scale inhibitor types have been used to hinder calcium carbonate scale [12][9–15]. The primary target of the chemical inhibitors is the calcium ion, which must be sequestered so it will not react with carbonate or bicarbonate ions, resulting in the prevention of calcium carbonate scale formation[18] [16–19]. Extensive inhibition studies have been completed on inhibitors derived from petrochemicals [22]. Hasson et al. mentioned that the most promising scale inhibitors are those derived from Polyaspartic acid (PASP) [23]. PASP is classified as a green inhibitor because it is non-nitrogenous, non-phosphorus, and biodegradable [22]. Martinod et al. studied the inhibition efficiency of PASP using chronoamperometry on synthetic brines that resembled those found in the North Sea, with a total amount of 14,224 ppm of Ca^{2+}. The author's findings indicated that 4 ppm PASP can reduce the amount of calcium carbonate deposition by more than 50%. Their study was completed at room temperature, which is not the case in water flooding oilfield processes where the temperature is high. A recent PASP study using static inhibition efficiency tests was performed by Liu et al. [24], who used diluted formation water

containing 253 ppm Ca^{2+} at 80°C. An inhibition efficiency percentage of 80% was achieved at those conditions with a dosage of 12 ppm PASP, which blocked the calcium carbonate crystal active sites [24]. These findings were also reported by Quan et al. [25], who employed the static bottle test to examine PASP performance on a synthetic water that contained 240 ppm Ca^{2+}. The authors reached a 90% inhibition at 30°C and 60ºC with 4 ppm and 12 ppm dosages, respectively. The development of PASP derived inhibitors may be attractive to oil and gas stakeholders; however, their current primary use is in water treatment processes. Polyepoxy succinic acid (PESA) is another green inhibitor used for calcium carbonate scale. Sun et al. utilized PESA in a static inhibition efficiency test at 30ºC. Their results indicated that 90% inhibition is reached with a dosage of 10 ppm and concentrations of 40, 100, and 200 ppm Ca^{2+} [26]. Liu et al. claimed that PESA's performance was better than PASP's; therefore, it may be a good alternative for water treatment technology [27]. Carboxymethyl inulin (CMI) is a biodegradable polymer that has been tested for calcium carbonate inhibition. Verraest et al. examined the performance of small CMI amounts, within a range of 0.1 to 200 ppm, on the crystallization and inhibition of calcium carbonate scale [28]. Verraest et al. concluded that CMI is a promising inhibitor since it changes the morphology of calcium carbonate crystals. Demandis et al. investigated CMI's performance by monitoring the formation of calcium carbonate scale with a scale sensor by measuring the absorbance, which agreed with studies completed by Verraest et al., indicating that a CMI dosage ranging from 100 to 300 ppm substantially decreased calcium carbonate scale formation. High CMI concentrations, approximately 1,000, ppm, dissolved large amounts of calcium carbonate scale. Kirboga et al. studied CMI's performance with a constant composition method to understand the growth rate of calcium carbonate crystals. In another recent study, Kirboga et al. performed experiments examining the effects of CMI on the morphology and polymorphs of crystallized calcium carbonate, reporting that CMI concentration ($2.5 \times 10{-}9$ to $25 \times 10{-}9$ mol/L) has the

greatest effect [29]. Qing Du et al. evaluated the performance of a natural polymer-based agent: starch-graft-poly-acrylic acid (St-g-PAA). St-g-PAA exhibited remarkable turbidity removal and effective efficiency results on calcium carbonate scale. The authors used the static bottle test with calcium and carbonate ion concentrations of 5 mmol/l. The inhibition efficiency was 94% at an optimal St-g-PAA dosage of 40 ppm with a test temperature of 70^{o}C [30]. Qiwei Wang et al. evaluated the performance of three different inhibitors: tri-phosphonate, penta-phosphonate, and polyacrylate-based chemicals. The authors examined the performance of the inhibitors in the presence of surfactants and polymers as enhanced oil recovery chemicals. Static bottle test experiments were conducted at 70^{o}C^{o} and a calcium ion concentration of 3,942 ppm [2]. The inhibition results for the tri-phosphonate and penta-phosphonate were greater when no EOR chemicals were present, reaching at least 80% with a dosage of 2 ppm [2]. Stéphanie C. de Morais et al. investigated the efficiency of sodium hexametaphosphate (SHMP) as a calcium carbonate inhibitor under static conditions at different temperatures, pressures, and SHMP concentrations. Their findings indicated an almost complete calcium carbonate inhibition at a pH of 6.5 and an SHMP dosage of 2.5 ppm. The calcium carbonate crystal deformation was confirmed with SEM images [31]. Yuwei Zuo et al. studied the calcium carbonate inhibition performance of carboxylic polymers with a low molecular weight. The authors used polyaspartic acid (PASA) and polyepxoysuccinic acid (PESA) to represent low molecular weight carboxylic polymers. PASA performed better than PESA, especially at normal temperatures. The author's findings were attributed to the high number of carboxylic groups in PASA compared to PESA [32]. Recently, the use of nanotechnology in oilfield scale inhibition has grown rapidly in both research and applications because of its effectiveness at different scaling environment[33]. Nanomaterials serve as a good inhibitors at high temperature and high pressure environments where scale is severe[34].

In this work, polyacrylamide functionalized nano-silica is synthesized and tested at different conditions.

Polyacrylamide (PAM) is widely used in the oil industry for enhanced oil recovery and is widely used as a flocculant in water treatment since it can bridge the particles that lead to the formation of aggregates with good settling properties [36,37]. The flocculation and adsorption capacity of PAM increases with increasing MW, branching, and charge density [38]. PAM hydrolysis results in the generation of more carboxylic groups at high temperatures, which act as Ca^{2+} adsorption or binding sites. Silica is known for its negative charge that acts as a nucleation site for calcium ions; therefore, PAM functionalized nanosilica was proposed as a calcium inhibitor since it has the dual advantage of carboxylic group chelation and enhanced silica nucleation. In addition, either high scale inhibitor dosages are needed for most of the inhibitors, or the inhibition efficiency is low according to the literature we reviewed. Furthermore, no comprehensive studies of the inhibition efficiency changes with temperature, pH, and CW/AW: cationic water/ anionic water were reported. Our proposed novel inhibitor will combine the advantages of Ca ion chelation caused by carboxylic groups on PAM and promote the Ca precipitation and nucleation caused by the negatively charged silica particles. Our proposed inhibitor was created using low-cost materials. The performance of the proposed system was evaluated and compared to typical commercial inhibitors. These performance and inhibitor dosages were evaluated to identify the optimal conditions for the pH, temperature, and brine concentrations relevant to oil and gas applications. In summary, this work aimed to focus on the synthesis and testing of a novel calcium carbonate scale inhibitor capable of withstanding high temperatures commonly encountered in the oil and gas industry. The thermal stability of the synthesized inhibitor was enhanced by nano-silica grafting. Another aim of the work was achieving higher efficiency at lower inhibitor dosages

ranges (0.2-2 ppm). Additionally, tests were to be performed under various key conditions such as different pH, and brine ratios (concentrations).

Experimental

2.1.1 Materials

All the chemicals used in the study were analytical grade. Hydrochloric acid, ethanol, sodium hydroxide, and potassium persulfate were obtained from BDH Chemicals limited, USA. Acrylic acid (AA), acrylamide (AM), and allyl chloride were supplied by Fluka Biochemika, USA. All chemicals were used without any further purification. Sodium sulfite and nano-silica were purchased from Sigma Aldrich (USA).

The chemical composition of the synthetic brine is listed in Table 1, representing the typical brine concentrations used for calcium carbonate inhibition tests [2]. The tested TDS is 66,530 ppm which is above the saturation limit and higher than what reported studies use (TDS of formation water of only 46,360 ppm) [35]. The synthetic brines were prepared using analytical grade chemicals and deionized water then filtered using 0.45 µm membrane filters. The inhibitor was tested at different conditions: temperatures of 25, 40, 60, and 80°C, and pH values of 7, and 9. Cationic and anionic brine ratios were varied from 50:50 to 80:20 and 20:80. The influence of the inhibitor's efficiency was monitored during these changes.

Table 1: Concentration of synthetic brine

Ion	Concentration (ppm)
Na^+	19,047
K^+	703
Mg_2^+	1,286
Ca_2^+	3,942
Sr_2^+	62
Cl^-	39,119
SO_4	1,847

HCO_3	500
TDS	66,530

2.1.2 Silica Precursor Preparation

The preparation of the silica precursor was accomplished using the established procedure based on a modified method by Liu et al. [36]. Silica (5 g) was treated with 50 ml hydrochloric acid (37%) for 12 hours to enrich its hydroxyl group, then filled and washed with excess DI water. This mixture was then refluxed with 50 ml of 0.04 M sodium hydroxide for 4 hours to transform the –OH silanol to an active negative charge. The activated silica was then reacted with allyl chloride at 60^{o}C for 24 hours, filtered, washed with deionized water and ethanol, and dried under a vacuum at 60^{o}C to generate an ethylene end group for use in free radical polymerization.

2.1.3 Polymer Synthesis

The as-prepared silica (2 g), 1.5 g of AA, and AM3 g of AM were mixed vigorously in a 500 ml three-necked flask and placed in an oil bath to undergo stirring for approximately 3 hours. Emulsification was performed by adding 0.05 g of sodium lauryl sulfate dissolved in 10 ml of DI water. The emulsified solution temperature was increased to 70^{o}C and stirred for 30 minutes before potassium persulfate (0.01 g in 10 ml of DI water) was added to initiate free radical polymerization. The polymerization reaction lasted for 3 hours, and the suspended material was recovered by filtration, precipitated in acetone, washed with DI water and ethanol, and dried at 60^{o}C for 10 hours to obtain the copolymer composite. A complete representation of the material preparation is presented in Figure 1.

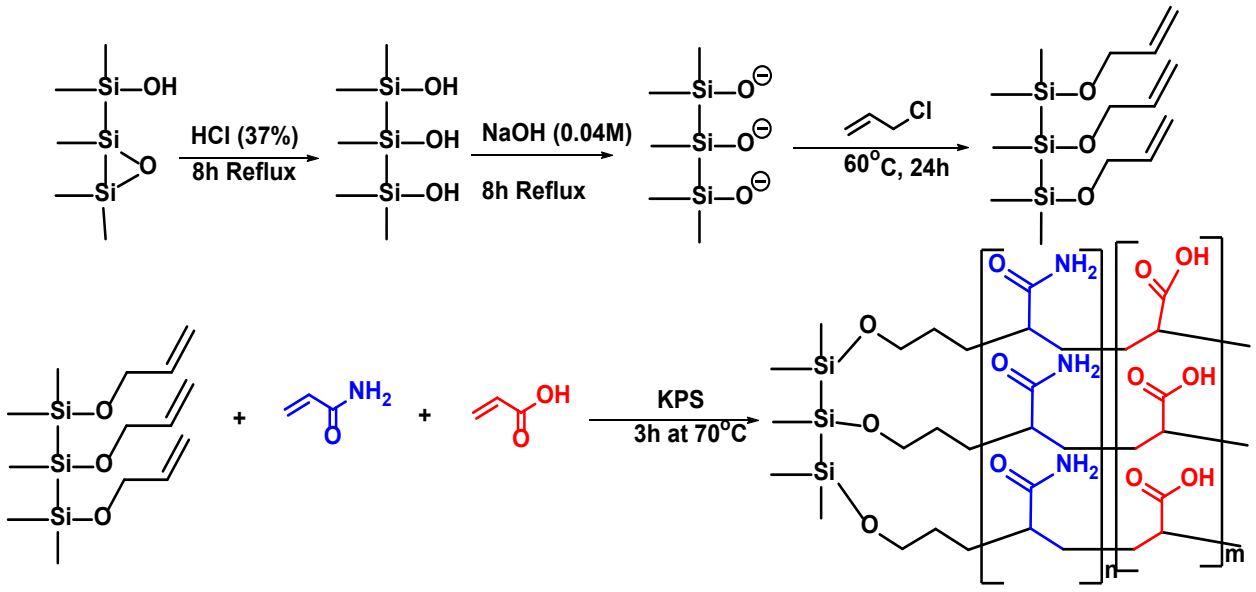

Figure 1: Schematics of PAM-SiO2NPs synthesis

2.2 Material Characterizations

2.2.1 Fourier Transform Infrared Spectroscopy

Field emission scanning electron microscopy (FE-SEM) (Lyra3 TESCAN) was used to characterize the surface characteristics of the PAM-SiO_2NPs. An X-ray Photoelectron spectroscopy (V.G. Scientific ESCALAB Mk (II) spectrometer with a non-monochromatic Al source (Kα, 1486.6 eV) was used to confirm the existence of elements on the sorbent surface. The FTIR spectra (Figure 2) were acquired with a Nicolet 6700 FT-IR (Thermo Electron Corporation) Fourier transform infrared spectroscope (FTIR). KBr was utilized to convert samples into pellets, and the spectrum was acquired with a resolution of 4 cm^{-1} by the assemblage of 32 scans within the range of 4000–400 cm^{-1}. A thermogravimetric study (SDT Q 600, TA Instruments, and New Castle, DE) was performed by heating the samples at increments with a frequency of 10◦C / minute up to 800◦C with a flow of nitrogen (75 ml/min).

The decrease in solid sample weight was recorded and investigated to measure the stability.

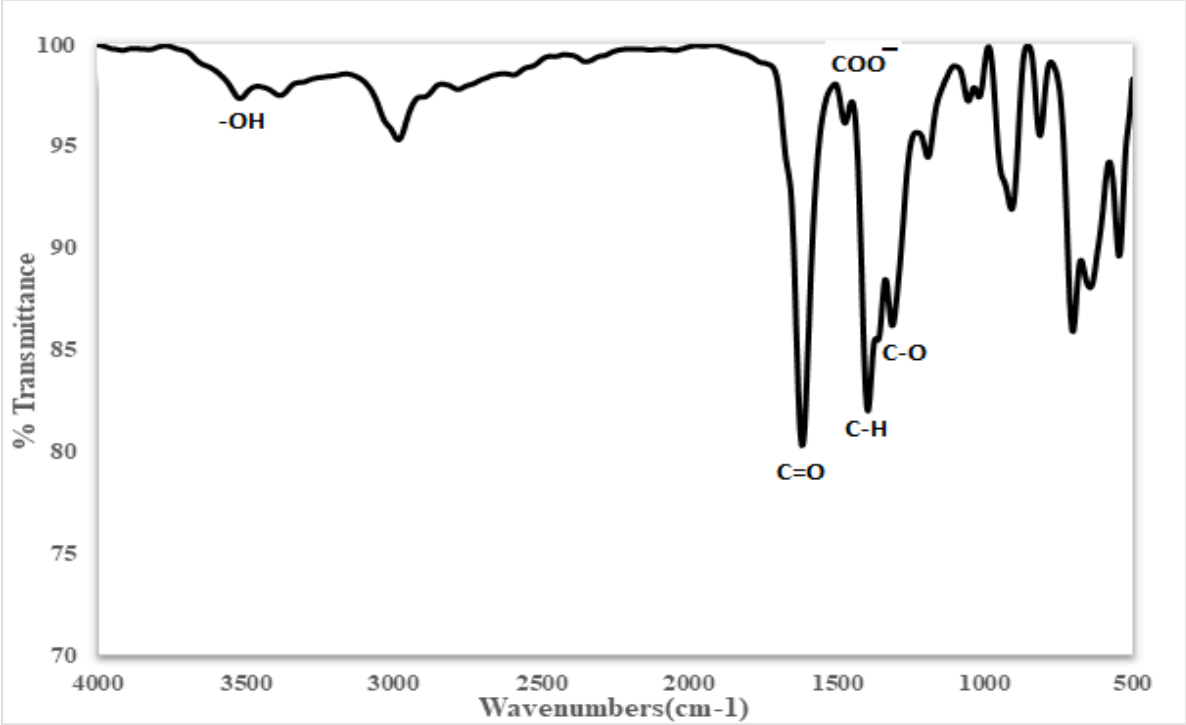

Figure 2: FTIR of PAM-SiO2NPs

The characteristic peak at approximately 1550 cm-1 is attributed to the carboxylic group COO^- [37]. The peak at 1,473 cm-1 corresponds to the $C-H$ bonds that are in the $C-H_2$ groups, while the peak at 2,984 cm-1 is attributed to the adsorbed surface molecules [36-37]. The peak at 3,500 cm^{-1} is an apparent characteristic of hydroxyl. The peak at 1,618.37 cm^{-1} is the characteristic peak of carbonyl, and those at 1,193 cm^{-1} and 1,057 cm^{-1} are attributed to the $C-O$ bond. Peaks at 1,396 cm^{-1} and 1,313 are characteristics of aromatic Skelton stretching vibrations, while the peaks at 910 cm^{-1} and 814.73 cm^{-1} are characteristics of the external plane bending vibration of CH_2 *and* CH double bond alkene. The weak peaks from 703.44 cm^{-1} to 546.71 cm^{-1} are due to amide linkage. All of the characteristic signals indicate the successful synthesis of the PAM-SiO_2NPs containing carboxyl and hydroxyl groups.

2.3.2 Thermogravimetric Analysis

An SDT Q600 model thermogravimetric analyzer was used to examine the thermal stability of the synthesized polymer material under a nitrogen atmosphere up to 800 °C, susceptible to a 20°C /minute heating ratio. The thermal properties of the polymer are represented in Figure 3. The weight of the polymer remained constant below 200 °C, then decreased dramatically as the temperature increased from 200°C to 400 °C, reaching a weight loss of approximately 60 % at 400 °C. The sharp drop at approximately around 400ºC is due to the breaking break of the C-C bond. The weight of the polymer decreased slightly at 400 °C as the temperature increased, approximately 30% at 800°C. The polymer possessed high thermal stability and could be used at temperatures up to 200°C, which is quite suitable for oil and gas reservoir conditions, which are usually within 100º-150ºC for oil and gas reservoirs, respectively.

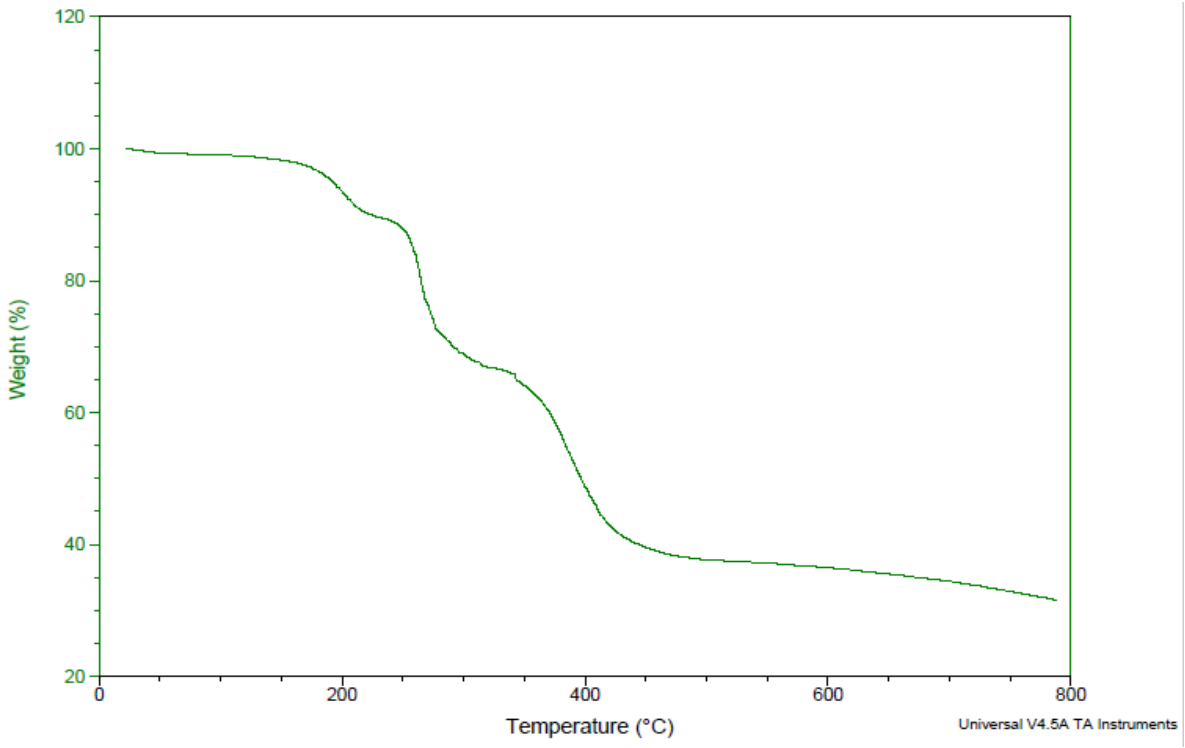

Figure 3: TGA curve of PAM-SiO2NPs

2.3.3 Nuclear Magnetic Resonance

The ^{1}H NMR and ^{13}C NMR spectra of the collected inhibitor product samples were obtained using a Bruker NMR 400 MHz spectrometer at room temperature and using D_2O as the solvent, with a dosage of 20-30 mg. Figure 4 illustrates the ^{1}H NMR and ^{13}C NMR spectra of PAM-SiO2NPs. The ^{1}H NMR signal at 4.70 ppm is the solvent residual peak of D_2O.

The characteristic peaks of the methine group (CH) appeared at 4.58 ppm in 1H NMR and 51.01 ppm in ^{13}C NMR. The characteristic peaks of the methylene group (CH_2) appeared at 2.65 ppm in ^{1}H NMR and 22.30 ppm in ^{13}C NMR. The 1H NMR signal at 1.24 ppm and the ^{13}C NMR signal at 19.49 ppm are assigned to the methyl group (CH_3). The characteristic peaks of the methine group associated with the carboxyl group (CHCOOH) appeared at 3.47 ppm in ^{1}H NMR and 60.56 ppm in ^{13}C NMR. The characteristic peaks of the methine group associated with the hydroxyl group (CHOH) appeared at 4.15 ppm in ^{1}H NMR and 65.93 ppm in ^{13}C NMR. The appearance of the methyl group, the methine group associated with the carboxyl group, and the hydroxyl group confirms the successful introduction of threonine. The ^{13}C NMR signals at 162.68, 171.05, 172.83, and 177.42 ppm are assigned to the four copolymer carbonyl groups of the copolymer [32-33]. All of the above characteristic signals demonstrate that PAM-SiO2NPs was successfully prepared.

2.3 Compatibility Test

It is critical to perform a compatibility test before an inhibition test since it ensures that the scale inhibitor will not cause problems, such as enhancing scale formation or phase separation, when added to the potential scale environment, especially at high concentrations. The synthetic brine was prepared by dissolving salts into DI water, the compositions of which are listed in Table 1. The oven was stabilized to the required test temperature of 80ºC after preparing the synthetic brine and adding it to 100 ml glass tubes. The brine was added to each glass bottle, with 50 ml in each

bottle. The inhibitor was then added using pipettes to achieve different concentrations: 10%, 1%, 0.1%, 100 ppm, and 10 ppm by volume. A blank sample was placed into the oven with no added inhibitor for each test. Visual inspections were recorded upon immediate injection of the inhibitor. The tubes were sealed and shaken vigorously, then placed in the oven. The product was compatible, as indicated in Figure 5.

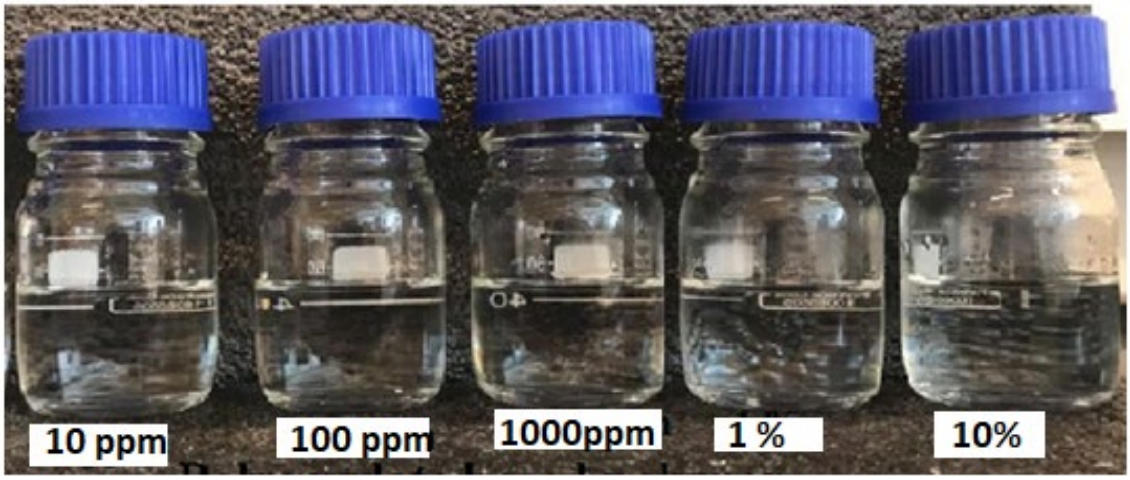

Figure 4: PAM-SiO2NPs compatibility test

2.4 Static Inhibition Test

A standard static inhibition test was performed under static conditions according to the petroleum industry standard of the People's Republic of China (SY/T 5673-93) as described in the literature [40][41], [42]. The cationic and anionic brines were prepared by dissolving the respective salts into DI water. The amounts of salts added (Table 2) were calculated to maintain the total composition listed in Table 1.

Table 2: Salts added for cationic water & anionic water preparation

Salt	CW (g)	AW(g)	MIX(g)
NaCl	7.93	14.92	24.56
KCl	0.67	-	0.67
$MgCl_2C.6H_2O$	5.38	-	5.38

$CaCl_2.2H_2OCO$	7.23	-	7.23
$NaHCO_3$	-	0.34	0.34
Na_2SO_4	-	1.37	1.37
pH	7.85	8.44	7.83

The ratio leading to the highest supersaturation and the ratio leading to the highest precipitation were tested to determine the scale inhibitor efficiency. The common practice, to test the ratio leading to the highest supersaturation. The required number of test bottles were labeled, corresponding to the sample's names provided for chemical analysis. Each test bottle was labeled using a permanent marker, indicating the name of the chemical and the dose rate. A 50 ml 'anion' solution was added to the six glass test bottles using the dispenser. This solution was also added to the blanks.

Each test bottle's 'anion' solution was dosed with the required amount of scale inhibitor intermediate solution using pipettes to reach the required final dose rate for each specific test. The concentrations tested in this study were 0.02 ppm, 0.1 ppm, 0.2 ppm, 2 ppm, and 20 ppm. The concentration of the inhibitor in the 'anion' solution was double that required for the test, which accounts for the dilution when mixed with the 'cation' solution. An inhibitor was not added to the 'blank' bottles.

An equal number of test bottles was prepared; each filled with 50 ml of the 'cation' solution using the dispenser. The test bottles were placed into a pre-heated oven at the appropriate test temperature for approximately 60 minutes to reach thermal equilibrium. The two brines were manually mixed by pouring the 'cation' solution into the 'anion' solution. The bottles were returned to the oven as soon as possible, and the timer was started at t_0. The test bottles were sampled at defined time intervals: 2, 16, and 24 hours. The pH values were monitored at the start of the test and upon cooling at the end. The samples taken at different time intervals were sent for

chemical analysis to evaluate the performance of the inhibitors. This procedure was performed in each experiment to evaluate the inhibitor at different conditions. The inhibitor was tested at 25 °C, 40°C, 60°C, and 80°C without altering the pH. The temperature was then set to 80°C, and the inhibitor was tested with pH values of 7, and 9. The test was performed at different CW/AW compositions: 80/20 and 20/80 by volume.

The inhibition efficiency, ε was calculated using the number of calcium ions remaining in the solution after the test using the following equation:

$$\varepsilon = \frac{C_2 - C_1}{C_0 - C_1}$$

Where C_2 is the Ca^{2+} (ppm) remaining in the filtrate after the reaction at different time intervals, $C_1$is the remaining Ca^{2+} (ppm) in the blank sample, and C_0 (ppm) is the concentration of Ca^{2+} (ppm) used before the test.

2.5 $CaCO_{3(s)}$ Characterization.

Samples of $CaCO_{3(s)}$ precipitate were collected by filtering the solutions of the blank and those with inhibitor dosages of 0.02 and 0.1 ppm using 0.45 µm membrane filters. The collected solid material was washed with DI water to remove potential contaminants, then dried overnight at 40°C before instrument characterization. The shape and surface morphology of the solid precipitate was examined with scanning electron microscopy (SEM). The collected sample's elemental composition was determined with Energy Dispersive X-Ray analysis (EDX). High-resolution images of the collected precipitate were completed with Transmission electron microscopy (TEM).

2. Results and discussion

3.1 Influence of Temperature on $CaCO_3$ Inhibition

The influence of temperature change on the efficiency of the inhibitor was tested at 25°C, 40°C, 60°C, and 80ºC. Temperature change was studied to investigate the inverse effect on calcium carbonate solubility even though it does not significantly affect efficiency. Aliquots of the test solutions, approximately 15 ml free from scale, were sampled and tested for Ca^{2+} ICP analysis at

t_0=2 hr. (used as the starting concentration for efficiency calculations) . , t_1=16 hr., and t_2= 24 hr. The results are reported in Figure 6.

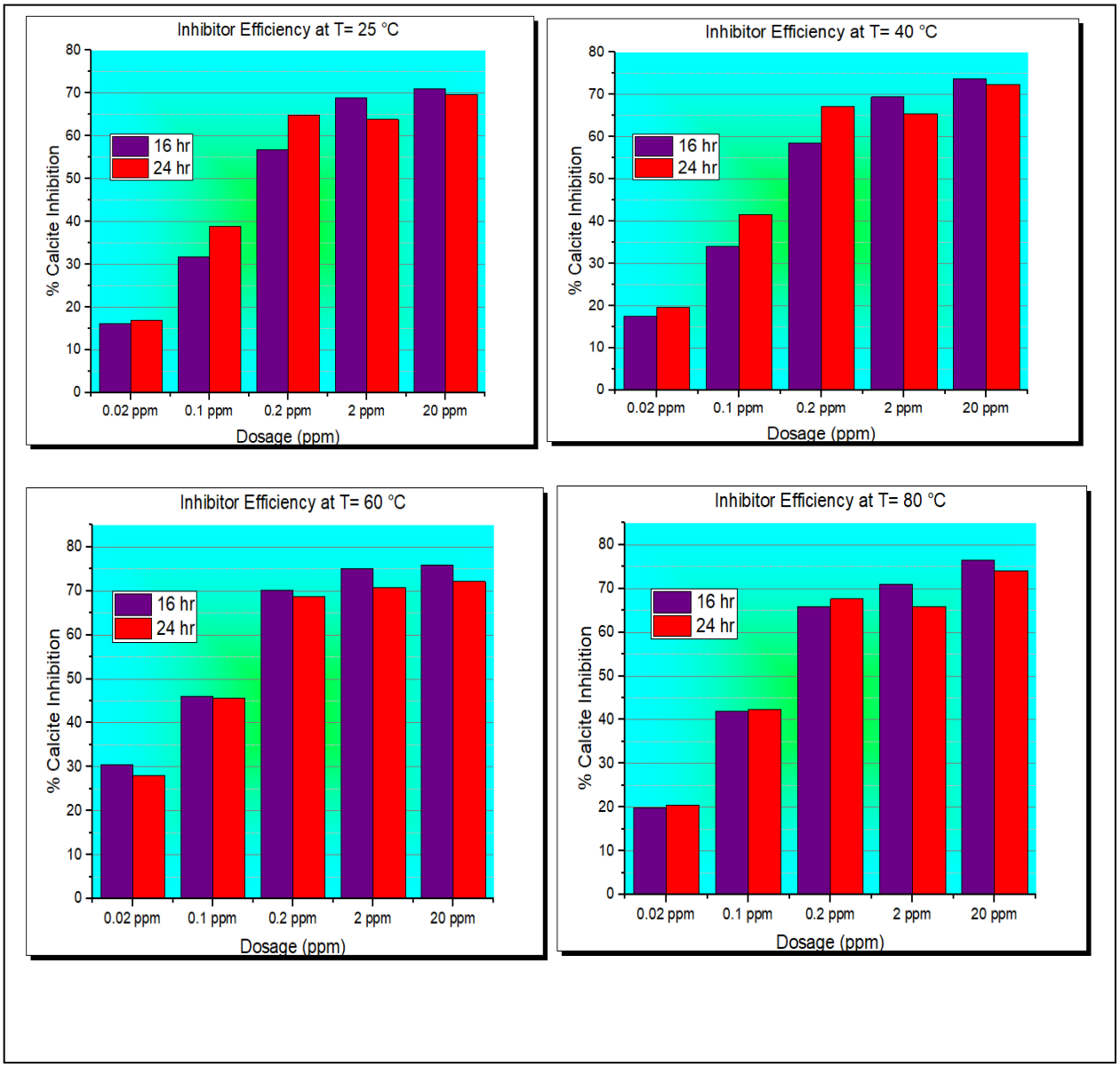

Figure 5: Influence of temperature on $CaCO_3$ inhibition

In addition, scale formation was faster and increases as the temperature increases due to the inverse solubility behavior of calcium carbonate which is in agreement with published literature[43], [44]. A minimal amount of scale was formed at 25°C, and the inhibitor efficiency only reached a maximum of 70% at the highest dosage (i.e. 20 ppm). A relatively large amount of scale formed as the temperature increased to 40°C, and the efficiency increased from approximately 20% using an inhibitor dosage of 0.02 ppm to approximately 75% using a dosage of 20 ppm. The inhibition

efficiency was further improved at 60°C where 30% inhibition was reached with an inhibitor dosage of 0.02 ppm, then to 76% using an inhibitor dosage of 20 ppm. The highest amount of scale formation occurred at 80ºC, where the inhibition efficiency increased from 20% at 0.02 ppm to approximately 77% at 20 ppm. The efficiency was higher after 16 hours of reaction at higher inhibitor dosages; while, the efficiency after 24 hours was higher with lower inhibitor dosages. This happens because at lower inhibitor concentration, the inhibitor does not interact with the formed scale whereby the crystal growth is not hindered, and scale continues to form, eventually enabling the inhibitor's function. The opposite occurs at higher inhibitor dosages where the inhibitor interacts with scale formation, leading to lower crystal growth after 16 hours. This phenomenon, explains how inhibition efficiency is higher at 16 hours than at 24 hours. The highest efficiencies recorded at 16 and 24 hours were at 20 ppm as summarized in table 3. The general trend of higher efficiencies at higher temperatures is explained by the endothermic chemisorption process of the inhibitor to the calcium carbonate crystals formed [45]. Hence, the adsorption is favored at high temperatures, facilitating the blockage and hindrance of calcium carbonate crystal growth.

Table 3: Highest Efficiencies Summary at 25 ^{o}C, 40 ^{o}C, 60 ^{o}C, and 80 ^{o}C.

T=25 ºC.		T=40 ºC.		T=60 ºC.		T=80 ºC.	
16 hr.	24 hr.	16 hr.	24 hr.	16 hr.	24 hr.	16 hr.	24 hr.
72%	70%	74%	72%	76%	72%	77%	74%

The functional groups of PAM-SiO2NPs explain the mechanism by which the inhibitor works: the amine group will chelate the calcium ions, mitigating scale formation by preventing them from forming carbonate and bicarbonate contacts. This chelation will produce water-soluble products since the nitrogen atom of the amine and the oxygen atom contain lone pairs and are electronegative.

3.2 Influence of pH on $CaCO_3$ Inhibition

Results from the examination of the influence of the pH on the calcium carbonate inhibition are summarized shown in Figure 7.

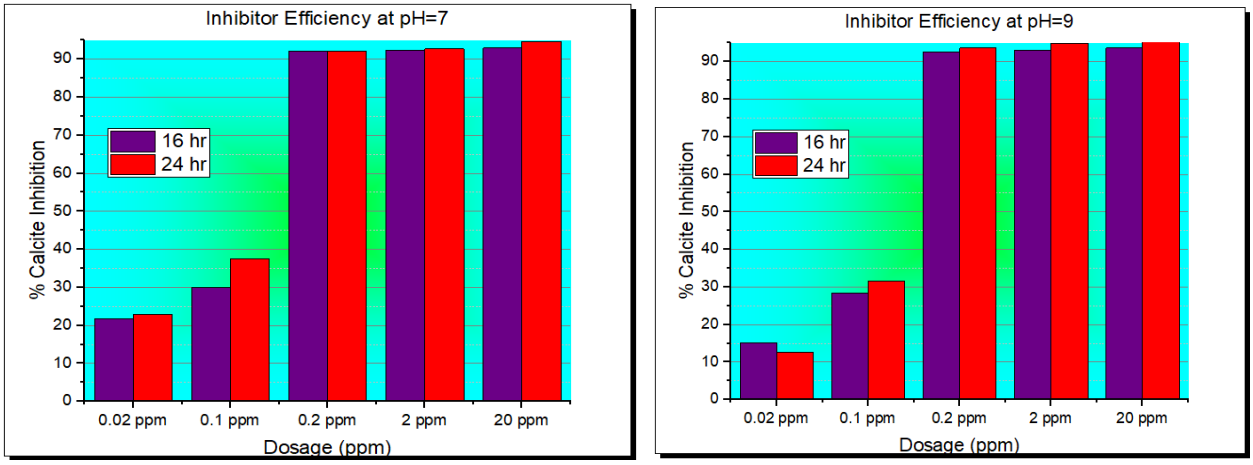

Figure 6: Influence of pH on $CaCO_3$ inhibition at different levels of inhibitor dosages

The test brines pH was 7.4, whereby one drop of 10% HCl was used to lower the pH to 7.0. Lowering the pH increased the inhibition efficiency to 94% with a 20 ppm dosage after 24 hours. The inhibition efficiency was only about 24% with an inhibitor dosage of 0.02 ppm. There was a slight increase (~ 13% at 24-hour test) in efficiency with an inhibitor dosage of 0.1 ppm followed by a substantial increase to over 90% with an inhibitor dosage of 0.2 ppm. The pH was then increased to 9 by adding 200 µL NaOH. The inhibition efficiency was slightly lower with a pH of 9 compared to a pH of 7, starting at 12% with an inhibitor dosage of 0.02 ppm, then increasing slightly to 31% with a 0.1 ppm dosage, followed by a sharp increase to greater than 90% efficiency for the higher dosages. The maximum efficiency attained was 95% with a 20 ppm dosage.

3.3 Influence of (CW/AW) Composition on $CaCO_3$ Inhibition

The influence of the cationic to anionic brine ratio was tested with two mixtures held at a steady temperature of 80°C with no change in pH. An 80 ml cationic brine and 20 ml anionic brine mixture was created with different inhibitor concentrations and one blank solution, the same setup we used for the other experiments. We also tested 20 ml cationic brine and 80 ml anionic brine mixtures. The results of this test are represented in Figure 8.

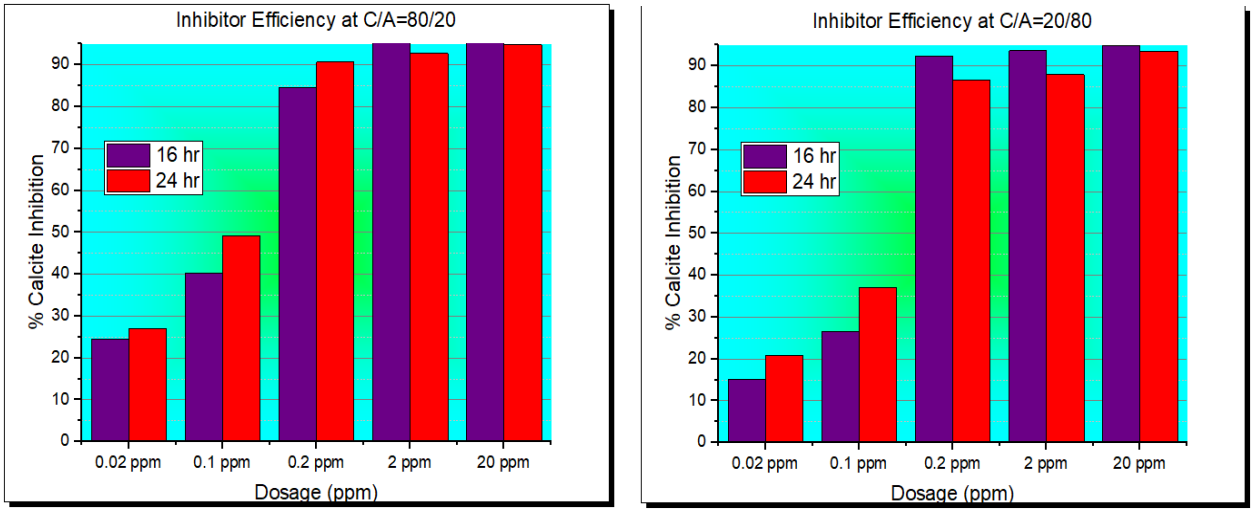

Figure 7: Influence of (CW/AW) composition on $CaCO_3$ inhibition

For the 24-hour test, the inhibition efficiency started around 25% with an inhibitor dosage of 0.02 ppm for the 80 ml cationic brine and 20 ml anionic brine mixture, increasing to about 49% efficiency with an inhibitor dosage of 0.1 ppm. The efficiency then increased to 95% at the highest inhibitor concentration, 20 ppm. The same behavior was observed for the 20 CW/80 AW ratio case, though the inhibition efficiency started at a lower value, 21% for the 0.02 ppm dosage and around 46% for the 0.1 ppm. This phenomenon is attributed to the higher number of calcium ions, which increases the potential for scale formation; therefore, the efficiency of the inhibitor was increased in the 80/20 ratio mixture.

The above results were compared with common calcium carbonate inhibitors published in the literature such as Polyaspartic acid (PASP) and pteroyl-l-glutamic acid (PGLU). Despite the high efficiency reported for PASP (95%) at 5 ppm, the efficiency is below 40% at 3 ppm[46]. Comparing to the proposed inhibitor in this study, PAM-SiO2NPs has relatively high efficiencies (> 80 %) even at low dosages up to 0.2 ppm. In addition, PAM-SiO2NPs has superior characteristics such as the high heat endurance capacity as seen from TGA in figure 3.

3.4 Investigation of Inhibition Mechanism

Scale samples collected after the static bottle test were characterized to further understand the chemistry behind $CaCO_3$ inhibition. SEM and EDS images in the presence and absence of PAM-SiO_2NPs are depicted in Figure 9.

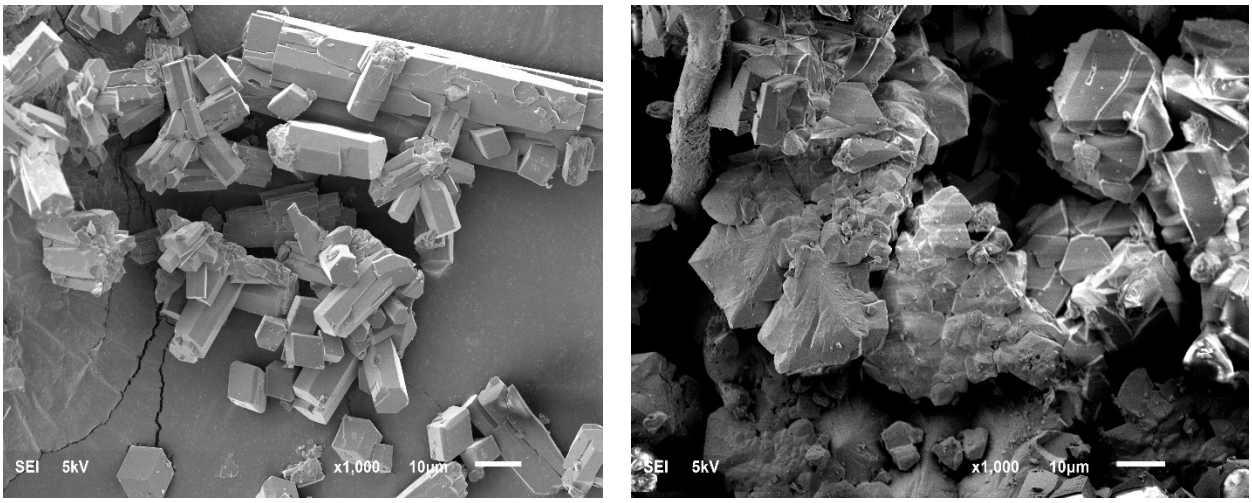

(a) (b)

Figure 8: SEM results of $CaCO_3$ precipitate (a) without inhibitor (b) with 0.1 ppm inhibitor

The amount of scale formation in the presence of the inhibitor was much less than the blank samples, especially at higher inhibitor dosages such as 0.1 ppm and 2 ppm. The SEM results for the calcium carbonate precipitate in the absence of the inhibitor exhibited regular aragonite structures of long strip crystals with a glassy surface that formed at elevated temperatures (Figure 9 (a)); however, crystals growth was interrupted with the absorption of the inhibitor onto the

crystal's surface, hindering the normal calcium carbonate crystal growth (Figure 9 (b)) [47]. The aragonite formation was consistent with findings from the literature since magnesium ions were present [34-35]. The rule of the inhibitor was designed to occupy the active crystal growth sites with the help of the functional groups, destroying the crystal lattice. The functional groups cause internal stress inside the crystals, leading to microcrystalline inhibition that prevents scale formation. The SEM characterization results indicate that in addition to calcium ion chelation, the inhibitor contributed to crystal growth distortion. Lower inhibitor concentrations did not significantly affect the crystals. Some crystal structures remained unchanged, especially with a dosage of 0.02 ppm. Energy Dispersive X-Ray analysis (EDX) was also performed to obtain information on the elements present in the scale sample (Figure 10).

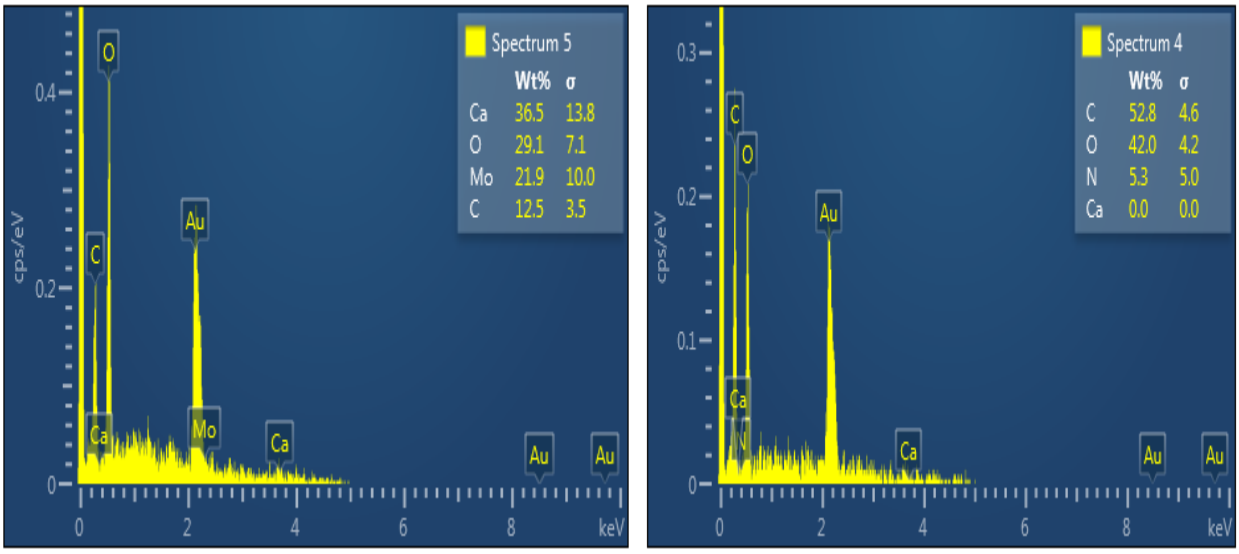

(a) (b)

Figure 9: EDS results of $CaCO_3$ precipitate (a) without inhibitor (b) at 0.1 ppm of inhibitor

The column-shaped structures formed in the blank samples (Figure 10 (a)) were developed into compact structures with inhibitor concentrations of 0.1 ppm. The columns were changed to distorted spheroid particles, and the packed structure evolved into loosely packed particles. Images of the formed scale were obtained with transmission electron microscopy (Figure 11).The images

are consistent with the SEM characterizations, supporting the inhibition mechanisms previously described.

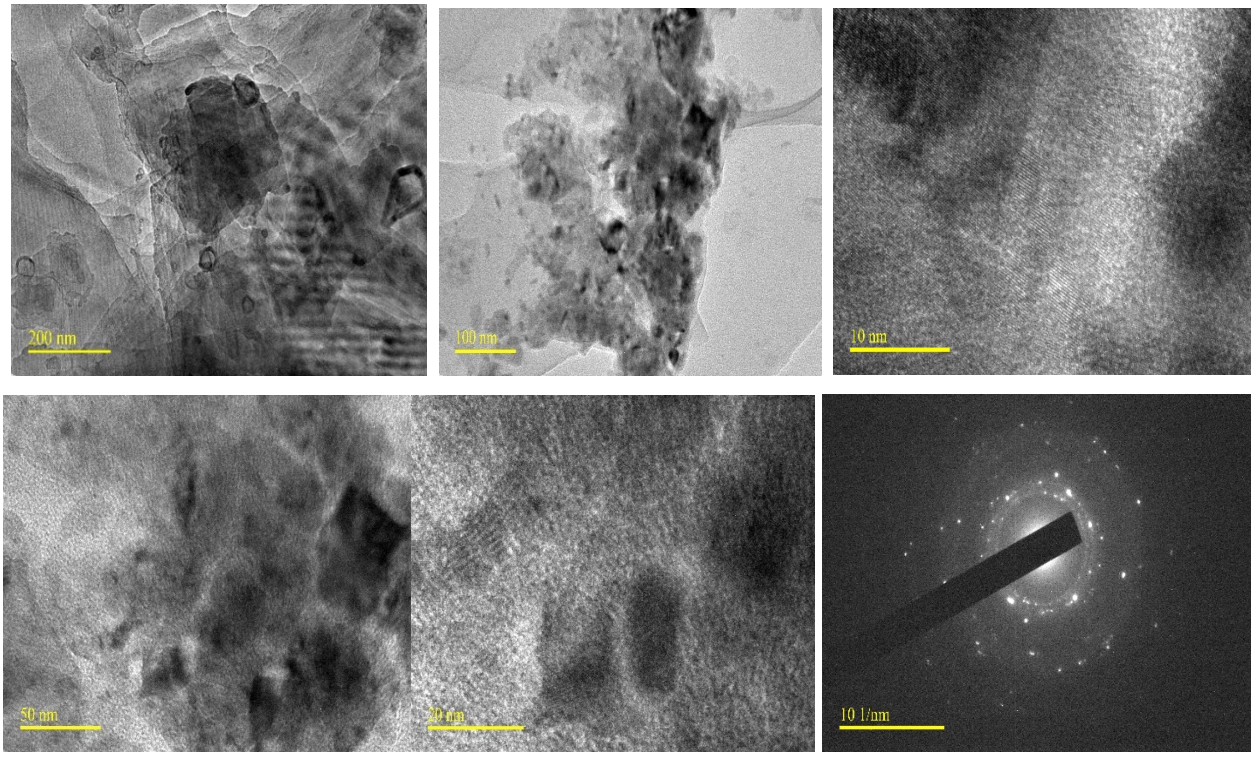

(a)

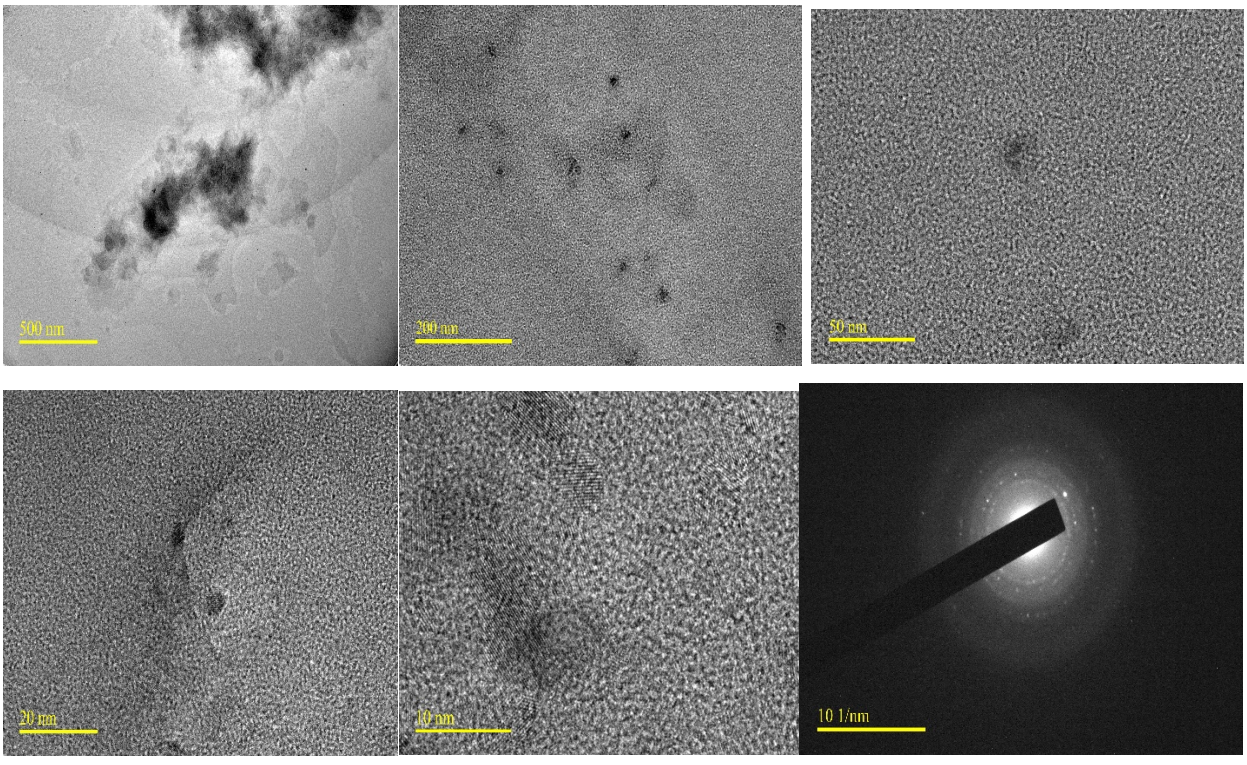

(b)

Figure 10: TEM of $CaCO_3$ precipitate (a) without inhibitor (b) at 0.1 ppm of inhibitor.

3. Conclusion

A novel PAM-SiO_2NPs polymer inhibitor have been successfully synthesized and characterized using FTIR, NMR, and TGA. The TGA results indicated that the inhibitor is thermally stable at elevated temperatures. FTIR and NMR results confirmed the successful synthesis of PAM-SiO_2NPs. Compatibility test shows that the inhibitor cause no precipitates or phase separations regardless of the concentration levels. The synthesized inhibitor was evaluated with static bottle tests under various conditions, such as changes in temperature, pH, and cationic to anionic brine ratios. The effectiveness of the inhibitor increased with temperature, reaching a peak at 80^{o}C. The influence of pH on the inhibitor efficiency revealed that as the pH increased, the inhibition efficiency increased. High inhibition efficiency was observed at higher temperatures and higher cationic to anionic ratio mixtures due to the inverse solubility behavior and the presence of more calcium ions that facilitate scale formation and, consequently, its inhibition. The inhibition collected scale samples were characterized by SEM, EDS, and TEM to further elucidate the inhibition mechanism. The characterization results revealed that in addition to the successful chelation of calcium by the inhibitor, the adsorption of the inhibitor on the active crystal growth sites hindered crystal growth, which improved inhibition efficiency. The results of this work demonstrate a promising potential for the inhibitor's efficiency at different temperatures, pH, and brine concentrations at relatively low inhibitor dosages.

5. **Acknowledgements**

We are grateful for the City of Grand Forks for funding this study through Project number: UND0023658.

References

[1] M. F. Mady and M. A. Kelland, "Overview of the Synthesis of Salts of Organophosphonic Acids and Their Application to the Management of Oilfield Scale," *Energy and Fuels*, vol. 31, no. 5, pp. 4603–4615, May 2017, doi: 10.1021/ACS.ENERGYFUELS.7B00708.

[2] Q. Wang *et al.*, "Laboratory study on efficiency of three calcium carbonate scale inhibitors in the presence of EOR chemicals," *Petroleum*, vol. 4, no. 4, pp. 375–384, 2018, doi: 10.1016/j.petlm.2018.03.003.

[3] H. Lu, B. Mccabe, J. Brooks, S. Heath, and S. Stevens, "A novel phosphonate scale inhibitor for scale control in ultra high temperature environments," in *Proceedings - SPE International Symposium on Oilfield Chemistry*, 2019, vol. 2019, doi: 10.2118/193554-ms.

[4] M. Nergaard and C. Grimholt, "An Introduction to Scaling causes , problems and solutions," no. november, 2010.

[5] H. Sojoudi *et al.*, "Micro-/Nanoscale Approach for Studying Scale Formation and Developing Scale-Resistant Surfaces," 2019, doi: 10.1021/acsami.8b18523.

[6] X. Wang, Q. Qu, S. Berry, J. Cutler, and B. Hughes, "SPE 165199 Iron Sulfide Removal : A Nonacidic Alternative to Hydrochloric Acid Treatment," 2013.

[7] J. Li, L. Chen, Y. Ye, and Z. Qi, "Solubility of CO2 in the Mixed Solvent System of Alkanolamines and Poly(ethylene glycol) 200," *J. Chem. Eng. Data*, vol. 59, no. 6, pp. 1781–1787, Jun. 2014, doi: 10.1021/JE400947T.

[8] Álvaro Pérez-Salado Kamps, Dirk Tuma, † and Jianzhong Xia, and G. Maurer*, "Solubility of CO2 in the Ionic Liquid [bmim][PF6]," *J. Chem. Eng. Data*, vol. 48, no. 3, pp. 746–749, May 2003, doi: 10.1021/JE034023F.

[9] A. R. Al Salami, A. A. Monem, Z. Development, and C. Zadco, "SPE 137906 Downhole

and Topside Scale Challenge ‘ Removal , Prevention and Inhibition Strategy ,’” 2010.

[10] M. El-said, M. Ramzi, and T. Abdel-moghny, “Analysis of oil fi eld waters by ion chromatography to determine the composition of scale deposition,” *DES*, vol. 249, no. 2, pp. 748–756, 2009, doi: 10.1016/j.desal.2008.12.061.

[11] A. Spinthaki *et al.*, “Searching for a universal scale inhibitor: A multi-scale approach towards inhibitor efficiency,” *Geothermics*, vol. 89, p. 101954, Jan. 2021, doi: 10.1016/j.geothermics.2020.101954.

[12] M. F. Mady, A. Rehman, and M. A. Kelland, “Synthesis and Study of Modified Polyaspartic Acid Coupled Phosphonate and Sulfonate Moieties As Green Oilfield Scale Inhibitors,” *Ind. Eng. Chem. Res.*, vol. 60, no. 23, pp. 8331–8339, Jun. 2021, doi: 10.1021/ACS.IECR.1C01473.

[13] Z. Xu, Y. Zhao, J. He, H. Qu, Y. Wang, and B. Wang, “Fouling characterization of calcium carbonate on heat transfer surfaces with sodium carboxymethyl cellulose as an inhibitor,” *Int. J. Therm. Sci.*, vol. 162, p. 106790, Apr. 2021, doi: 10.1016/j.ijthermalsci.2020.106790.

[14] Y. Zuo, W. Yang, K. Zhang, Y. Chen, X. Yin, and Y. Liu, “Experimental and theoretical studies of carboxylic polymers with low molecular weight as inhibitors for calcium carbonate scale,” *Crystals*, vol. 10, no. 5, p. 406, May 2020, doi: 10.3390/cryst10050406.

[15] M. Zhou, Y. Gu, R. Yi, and H. Han, “Synthesis and property study of ter-copolymer P(MA-AMPS-HPA) scale inhibitor,” *J. Polym. Res.*, vol. 27, no. 10, pp. 1–12, Oct. 2020, doi: 10.1007/s10965-020-02270-7.

[16] M. Chaussemier *et al.*, “State of art of natural inhibitors of calcium carbonate scaling. A review article,” *Desalination*, vol. 356. Elsevier B.V., pp. 47–55, Jan. 05, 2015, doi: 10.1016/j.desal.2014.10.014.

[17] M. Boumagoura, S. Ghizellaoui, S. Rhouati, H. Cheap-Charpentier, and O. Horner, "Calcium carbonate scaling prevention by a green chemical inhibitor, gallic acid," *Water Environ. J.*, 2021, doi: 10.1111/wej.12690.

[18] Z. Zhang, P. Zhang, Z. Li, A. T. Kan, and M. B. Tomson, "Laboratory Evaluation and Mechanistic Understanding of the Impact of Ferric Species on Oilfield Scale Inhibitor Performance," *Energy & Fuels*, vol. 32, no. 8, pp. 8348–8357, Aug. 2018, doi: 10.1021/ACS.ENERGYFUELS.8B01837.

[19] A. Spinthaki *et al.*, "A universal scale inhibitor: A dual inhibition/dispersion performance evaluation under difficult brine stresses," *Geothermics*, vol. 89, p. 101972, Jan. 2021, doi: 10.1016/j.geothermics.2020.101972.

[20] E. Khamis, D. E. Abd-El-Khalek, M. A. Abdel-Kawi, and J. M. Anwar, "Scale inhibition in industrial water systems using chitosan-alginate mixture," *Water Environ. J.*, 2021, doi: 10.1111/wej.12704.

[21] A. Khormali, G. Bahlakeh, I. Struchkov, and Y. Kazemzadeh, "Increasing inhibition performance of simultaneous precipitation of calcium and strontium sulfate scales using a new inhibitor — Laboratory and field application," *J. Pet. Sci. Eng.*, vol. 202, p. 108589, Jul. 2021, doi: 10.1016/j.petrol.2021.108589.

[22] M. Chaussemier *et al.*, "State of art of natural inhibitors of calcium carbonate scaling. A review article," *Desalination*, vol. 356, pp. 47–55, Jan. 2015, doi: 10.1016/j.desal.2014.10.014.

[23] F. Hasson and S. Keeney, "Enhancing rigour in the Delphi technique research," *Technol. Forecast. Soc. Change*, vol. 78, no. 9, pp. 1695–1704, Nov. 2011, doi: 10.1016/j.techfore.2011.04.005.

[24] M. Liu, H. Su, and T. Tan, "Synthesis and properties of thermo- and pH-sensitive poly(N-

isopropylacrylamide)/polyaspartic acid IPN hydrogels," *Carbohydr. Polym.*, vol. 87, no. 4, pp. 2425–2431, Mar. 2012, doi: 10.1016/j.carbpol.2011.11.010.

[25] Z. Quan, Y. Chen, X. Wang, C. Shi, Y. Liu, and C. Ma, "Experimental study on scale inhibition performance of a green scale inhibitor polyaspartic acid," *Sci. China, Ser. B Chem.*, vol. 51, no. 7, pp. 695–699, Jul. 2008, doi: 10.1007/s11426-008-0063-y.

[26] Y. SUN, W. XIANG, and Y. WANG, "Study on polyepoxysuccinic acid reverse osmosis scale inhibitor," *J. Environ. Sci.*, vol. 21, no. SUPPL. 1, 2009, doi: 10.1016/S1001-0742(09)60041-3.

[27] L. Liu *et al.*, "Fatigue and sleep quality are associated with changes in inflammatory markers in breast cancer patients undergoing chemotherapy," *Brain, Behavior, and Immunity*, vol. 26, no. 5. pp. 706–713, Jul. 2012, doi: 10.1016/j.bbi.2012.02.001.

[28] D. L. Verraest, J. A. Peters, H. van Bekkum, and G. M. van Rosmalen, "Carboxymethyl inulin: A new inhibitor for calcium carbonate precipitation," *J. Am. Oil Chem. Soc.*, vol. 73, no. 1, pp. 55–62, Jan. 1996, doi: 10.1007/BF02523448.

[29] S. Kirboga and M. Öner, "The inhibitory effects of carboxymethyl inulin on the seeded growth of calcium carbonate," *Colloids Surfaces B Biointerfaces*, vol. 91, no. 1, pp. 18–25, Mar. 2012, doi: 10.1016/j.colsurfb.2011.10.031.

[30] T. D. Baugh, J. Y. Lee, K. Winters, J. Waters, and J. Wilcher, "A fast and information-rich test method for scale inhibitor perfomance," in *Offshore Technology Conference, Proceedings*, 2012, vol. 2, pp. 1104–1113, doi: 10.4043/23150-ms.

[31] S. C. de Morais *et al.*, "Effect of pH on the efficiency of sodium hexametaphosphate as calcium carbonate scale inhibitor at high temperature and high pressure," *Desalination*, vol. 491, Oct. 2020, doi: 10.1016/j.desal.2020.114548.

[32] Y. Zuo, W. Yang, K. Zhang, Y. Chen, X. Yin, and Y. Liu, "Experimental and Theoretical

Studies of Carboxylic Polymers with Low Molecular Weight as Inhibitors for Calcium Carbonate Scale," *Crystals*, vol. 10, no. 5, p. 406, May 2020, doi: 10.3390/cryst10050406.

[33] M. F. Mady and M. A. Kelland, "Review of Nanotechnology Impacts on Oilfield Scale Management," *ACS Appl. Nano Mater.*, vol. 3, no. 8, pp. 7343–7364, Aug. 2020, doi: 10.1021/ACSANM.0C01391.

[34] A. Sheikhi, A. L. J. Olsson, N. Tufenkji, A. Kakkar, and T. G. M. Van De Ven, "Overcoming Interfacial Scaling Using Engineered Nanocelluloses: A QCM-D Study," 2018, doi: 10.1021/acsami.8b07435.

[35] O. S. Sanni, O. Bukuaghangin, T. V. J. Charpentier, and A. Neville, "Evaluation of laboratory techniques for assessing scale inhibition efficiency," *J. Pet. Sci. Eng.*, vol. 182, p. 106347, Nov. 2019, doi: 10.1016/J.PETROL.2019.106347.

[36] X. Liu, K. Liu, S. Gou, L. Liang, C. Luo, and Q. Guo, "Water-Soluble Acrylamide Sulfonate Copolymer for Inhibiting Shale Hydration," 2014, doi: 10.1021/ie403956d.

[37] Z. Zhu, M. Li, and E. Jin, "Effect of an allyl pretreatment of starch on the grafting efficiency and properties of allyl starch- *g* -poly(acrylic acid)," *J. Appl. Polym. Sci.*, vol. 112, no. 5, pp. 2822–2829, Jun. 2009, doi: 10.1002/app.29621.

[38] X. J. Zhang, T. Y. Ma, and Z. Y. Yuan, "Titania-phosphonate hybrid porous materials: Preparation, photocatalytic activity and heavy metal ion adsorption," *J. Mater. Chem.*, vol. 18, no. 17, pp. 2003–2010, Apr. 2008, doi: 10.1039/b717060b.

[39] T. Z. Ren, Z. Y. Yuan, and B. L. Su, "Surfactant-assisted preparation of hollow microspheres of mesoporous TiO2," *Chem. Phys. Lett.*, vol. 374, no. 1–2, pp. 170–175, Jun. 2003, doi: 10.1016/S0009-2614(03)00722-X.

[40] X. Liu, X. Sheng, Q. Yao, L. Zhao, Z. Xu, and Y. Zhou, "Synthesis of a New Type of 2-Phosphonobutane-1,2,4-tricarboxylic-Acid-Modified Terpolymer Scale Inhibitor and Its

Application in the Oil Field," 2021, doi: 10.1021/acs.energyfuels.1c00167.

[41] Q. Wang, W. Al-Nasser, T. C. Saudi, A. Dhahran, S. Arabia, and F. Liang, "CALCIUM CARBONATE SCALE INHIBITION: EFFECTS OF EOR CHEMICALS," OnePetro, Apr. 2018. Accessed: Jul. 07, 2021. [Online]. Available: http://onepetro.org/NACECORR/proceedings-pdf/CORR18/All-CORR18/NACE-2018-10546/1186452/nace-2018-10546.pdf.

[42] Q. Wang *et al.*, "Inhibition of calcium carbonate scale in the presence of EOR chemicals," in *Proceedings - SPE International Symposium on Oilfield Chemistry*, Apr. 2017, vol. 2017-April, pp. 333–346, doi: 10.2118/184534-ms.

[43] R. Ketrane, B. Saidani, O. Gil, L. Leleyter, and F. Baraud, "Efficiency of five scale inhibitors on calcium carbonate precipitation from hard water: Effect of temperature and concentration," *Desalination*, vol. 249, no. 3, pp. 1397–1404, Dec. 2009, doi: 10.1016/j.desal.2009.06.013.

[44] X. Li *et al.*, "Effect of six kinds of scale inhibitors on calcium carbonate precipitation in high salinity wastewater at high temperatures," *J. Environ. Sci. (China)*, vol. 29, pp. 124–130, Mar. 2015, doi: 10.1016/j.jes.2014.09.027.

[45] E. Kurtulbaş, E. Yıldırım, S. Emik, and S. Şahin, "A detailed study on the sorption characteristics of humic acid onto calcined dolomite," *J. Mol. Struct.*, vol. 1219, Nov. 2020, doi: 10.1016/J.MOLSTRUC.2020.128606.

[46] Z. Liu, Y. Sun, X. Zhou, T. Wu, Y. Tian, and Y. Wang, "Synthesis and scale inhibitor performance of polyaspartic acid," *J. Environ. Sci.*, vol. 23, no. SUPPL., pp. S153–S155, Jun. 2011, doi: 10.1016/S1001-0742(11)61100-5.

[47] S. Naserifar, S. Zybin, C.-C. Ye, and W. A. G. Iii, "trioxide (MTO3N) green energetic materials from DFT and ReaxFF molecular modeling †," 2016, doi: 10.1039/c5ta06426k.

[48] G. Liu *et al.*, “Scale Inhibition by a Carboxylate-Terminated Double-Hydrophilic Block Copolymer in Industrial Recycling Water,” *J. Water Chem. Technol.*, vol. 41, no. 2, pp. 73–80, 2019, doi: 10.3103/s1063455x19020024.

[49] Z. Kiaei and A. Haghtalab, “Experimental study of using Ca-DTPMP nanoparticles in inhibition of CaCO3 scaling in a bulk water process,” *Desalination*, vol. 338, no. 1, pp. 84–92, 2014, doi: 10.1016/j.desal.2014.01.027.